JMEPEG
https://doi.org/10.1007/s11665-024-09827-3

1059-9495/$19.00

ORIGINAL RESEARCH ARTICLE

The Effect of Precipitate Phases on Mechanical Properties of Al-Cu Alloys at Elevated Temperatures

Zhihao Bai, Ganghui Wu, Dinghong You, Jian Wang, and Dongshuai Zhou

Submitted: 15 November 2023 / Revised: 2 April 2024 / Accepted: 20 May 2024

The tensile deformation behaviors of the inoculated Al-Cu alloys were examined through uniaxial tensile tests conducted within a temperature range of (433-493) K and strain-rate range of (10^{-4}-10^{-1}) s^{-1}. After tensile tests, an investigation was carried out to analyze the changes of the θ′ precipitate phases with deformation behaviors. The findings suggest that the growth of θ′ precipitates is inversely proportional to the strain rates or directly proportional to the deformation temperatures, leading to a decrease in work-hardening ability during plastic deformation and subsequently reduce the level of flow stress. Moreover, the deformation mechanism of the investigated Al-Cu alloy at elevated temperatures is controlled by dislocation creep.

Keywords constitution equation, flow stress, metals and alloys, precipitate phases

1. Introduction

Precipitation strengthening plays a crucial role in enhancing the strength of Al alloys. The enhanced strength improvement is closely linked to the characteristics of precipitates, including their structure, shape, size and number density (Ref 1-5). In Al-Cu alloys, the precipitation sequence can generally be described as follows: starting with a supersaturated solid solution, followed by the formation of Guinier–Preston (G.P.) I zone and θ″ (G.P. II zone), leading to θ′ phase and finally θ phase (Ref 6-8). The relationships of the θ″, θ′ and θ phases with α-Al matrix phase are coherent, semi-coherent and noncoherent, respectively. Among the various forms of precipitation, the plate-like θ′ phase is widely recognized as the most effective strengthening component in Al-Cu alloys. This phase possesses a body-centered tetragonal structure and typically precipitates along the {100}α-Al planes. The presence of abundant θ′ phases in Al-Cu alloys significantly enhances their strength at room temperature through precipitation strengthening. However, this effect will be weakened at higher temperatures due to the coarsening of the θ′ phase. Therefore, it is very necessary to improve thermal stability of θ′ phase so as to enhance the mechanical properties of the Al-Cu alloy at elevated temperatures (Ref 9-24).

Li (Ref 10) investigated the effect of microalloying elements (Zr, V and Sc) additions on thermal stability of precipitates and elevated temperature properties of Al-Cu 224 cast alloys. They found that Zr, V and Sc can delay the transformation from θ″ to θ′ after T7 heat treatment and improved the thermal stability of θ′ phases when exposed to temperatures as high as 300 °C for 100 h after T7A heat treatment. Hu (Ref 012, 13) found that when addition Mg microalloying into Al-Cu 224 cast alloys, the creep, low cycle fatigue and thermomechanical fatigue behaviors can be improved, which is because Mg element can increased higher thermal stability of θ′ precipitates. According to Shyam et al.'s study (Ref 16), introducing Mn or Zr elements into interfaces could potentially enhance thermal stability within θ' phase structures. Consequently, this leads to increase structural stability even when exposed to temperatures as high as 350 °C, resulting in notable improvements in elevated temperature strength for Al-Cu alloys. In addition, Chen et al. (Ref 17) revealed that Au additions significantly reduce the nucleation energy barrier of θ′ phase, and simultaneously increase the low-temperature age hardening of Al-Cu alloy. Besides, rare earth elements have also been shown to accelerate both precipitate nucleation and growth of θ' phases, resulting in significant improvements in creep resistance for Al-Cu alloys (Ref 21-24). Recently, there have been reported on the enhancement of high-temperature properties of Al-Cu alloys inoculated by metallic glasses (Ref 25-27). However, there is a lack of detailed investigation into the changes of the θ′ phase in the new type of Al-Cu alloys at elevated temperatures. Therefore, this paper aims to discuss the impact of precipitate phases on the mechanical properties of Al-Cu alloys under high temperatures conditions.

In this study, the hot tensile tests of the Al-Cu alloys inoculated by Zr-based metallic glass were investigated. The tests were carried out at various temperatures ranging from 433 to 493 K and strain rates between 10^{-4} and 10^{-1} s^{-1}. The relation between θ′ phase and mechanical properties at elevated temperatures was discussed in detailed.

Zhihao Bai, Ganghui Wu, Dinghong You, and **Dongshuai Zhou**, Department of Materials and Engineering, Jiangsu University of Technology, No. 1801 Zhongwu Street, Changzhou 213001, China; **Jian Wang**, Department of Materials and Engineering, Jiangsu University of Technology, No. 1801 Zhongwu Street, Changzhou 213001, China; and College of Mechanical and Electrical Engineering, Hohai University, Changzhou 213022, China. Contact e-mail: zhbai123@sina.com.

Published online: 23 July 2024

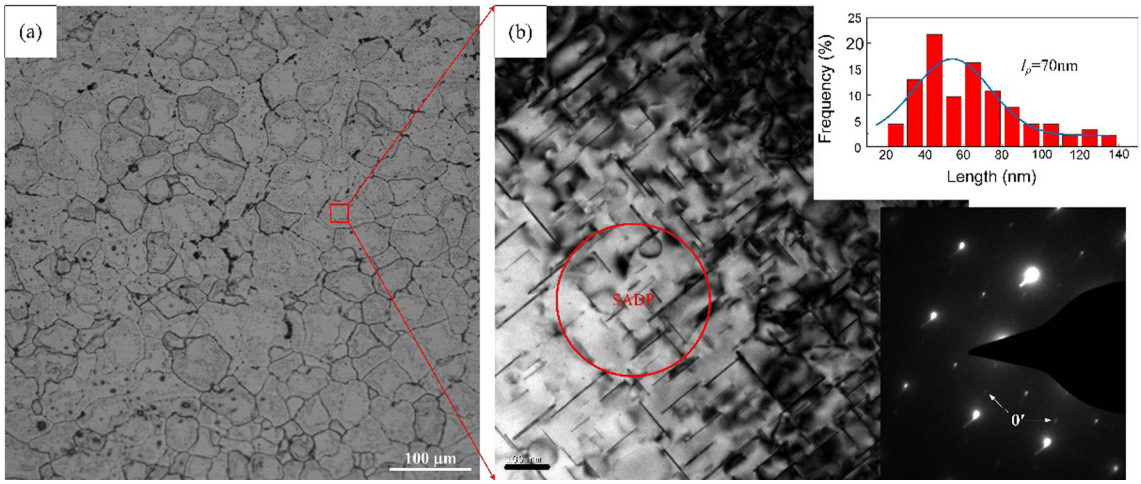

Fig. 1 Microscopy graph of the studied Al-Cu alloy: (a) optical micrograph and (b) TEM micrograph

2. Experimental

The present study utilized an Al-Cu alloy, which consisted of 5.0 wt.% Cu, 0.45 wt.% Mn, 0.30 wt.% Ti, 0.15 wt.% V, 0.15 wt.% Zr and trace amounts (0.004 wt.%) of B with the remaining balance being Al. To enhance its properties, the alloy was inoculated with a Zr-based metallic glass following the procedure described in reference (Ref 23). Subsequently, T6 heat treatment (solution at 811 K for 10 h and aging at 438 K for 10 h) was performed on the Al-Cu alloy. The microstructure analysis involved examination using both Zeiss optical microscope (Axio Imager) and high-resolution transmission electron microscopy (HRTEM) equipment model JEM-2100F from Japan as depicted in Fig. 1. The microstructure characterization revealed that the Al-Cu alloy is composed of primarily α-Al phase along with undissolved Al_2Cu phase located at grain boundaries and small θ' precipitates dispersed within the grains measuring approximately an mean length of about 70 nm. According to reference literature (Ref 10), true diameter d_p of precipitate phases can be mathematically represented as: $d_p = \frac{2(l_p-t)+2\sqrt{(l_p-t)^2+\pi l_p t}}{\pi}$ (l_p is the measured mean length, and t is the thickness of foil.

The tensile tests were performed using dog-bone-shaped samples, which had a gauge cross section measuring 5.0 × 2.5 mm and a gauge length of 30.0 mm. These tests were conducted on a servo-hydraulic materials testing system (INSTRON, 5869, England). The tensile tests were conducted under four different temperatures (433, 453, 473 and 493 K) and four different strain rates (10^{-4}, 10^{-3}, 10^{-2}, 10^{-1} s^{-1}). In order to obtain the heat balance, each sample was held for 10 min at isothermal conditions of the setting temperature before the tensile tests. After hot tensile test, the samples were examined by TEM.

3. Results and Discussion

3.1 High-Temperature Deformation Behavior

Figure 2 shows the stress–strain behaviors of the Al-Cu alloys investigated in this study at different temperatures ranging from 433 to 493 K, and with various strain rates between 10^{-4} and 10^{-1} s^{-1}. The detailed results of the tensile tests can be found in Table 1. During plastic deformation, as the strain increases, the flow stress initially exhibits a rapid rise until it reaches its peak value (σ_p), followed by a gradual decrease until fracture occurs. It was observed that higher strain rates or lower deformation temperatures led to an increase in peak stress, while lower strain rates or higher deformation temperatures resulted in a decrease in peak stress. These findings highlight the significant influence of temperature and strain rate on flow stress under all tested conditions. As reported by Ref 26, it is evident that the mechanical properties of these Al-Cu alloys are significantly superior compared to uninoculated Al-Cu alloys under same testing conditions, and approximately equivalent to those inoculated alloys by Ni-Base metallic glass. Figure 3 shows a typical SEM fractography of the studied Al-Cu alloy after tensile experiments. It can be clearly observed that the small uniform dimples are uniformly distributed on the fracture surface, indicating that the fracture mode was mainly ductile fracture. However, comparing the fracture morphology of low strain rate and high strain rate, it is obvious that the fracture has a trend of intergranular fracture at low strain rate. This is because lower strain rate allows sufficient time for softening along grain boundaries during plastic deformation stage; consequently, leading cracks develop along these boundaries. In particular, it is worth noting that the elongation of Al-Cu alloy under 493K and 10^{-1} s^{-1} dropped sharply to 4.36%.

Figure 4 shows a typical TEM micrograph of θ′ precipitates observed after conducting tensile tests. Under strain rates of 10^{-4} and 10^{-1} s^{-1} at a temperature of 433K, the sizes of θ′ precipitates were calculated to be 105.5 and 100.4 nm, respectively. Similarly, at a temperature of 493 K, the sizes were found to be 121.1 and 111.1 nm under strain rates of 10^{-4} and 10^{-1} s^{-1}, respectively. The change in size of θ′ precipitates can be approximatively described using the Ostwald Ripening equation $D_1^2 - D_0^2 = K\tau$ (where D_1 represents the mean size after tensile test, D_0 represents the mean size before test, K is a material-dependent constant, and τ is time). According to the Ostwald Ripening equation, the values of K are 3.0, 13.5, 10.4 and 26.1 under strain rates 10^{-4} s^{-1} at 433 K, strain rates 10^{-1} s^{-1} at 433 K, strain rates 10^{-4} s^{-1} at 493 K and strain rates 10^{-1} s^{-1} at 493 K, respectively. At both temperatures (433 and 493 K), under strain rates of 10^{-4} s^{-1}, K values are

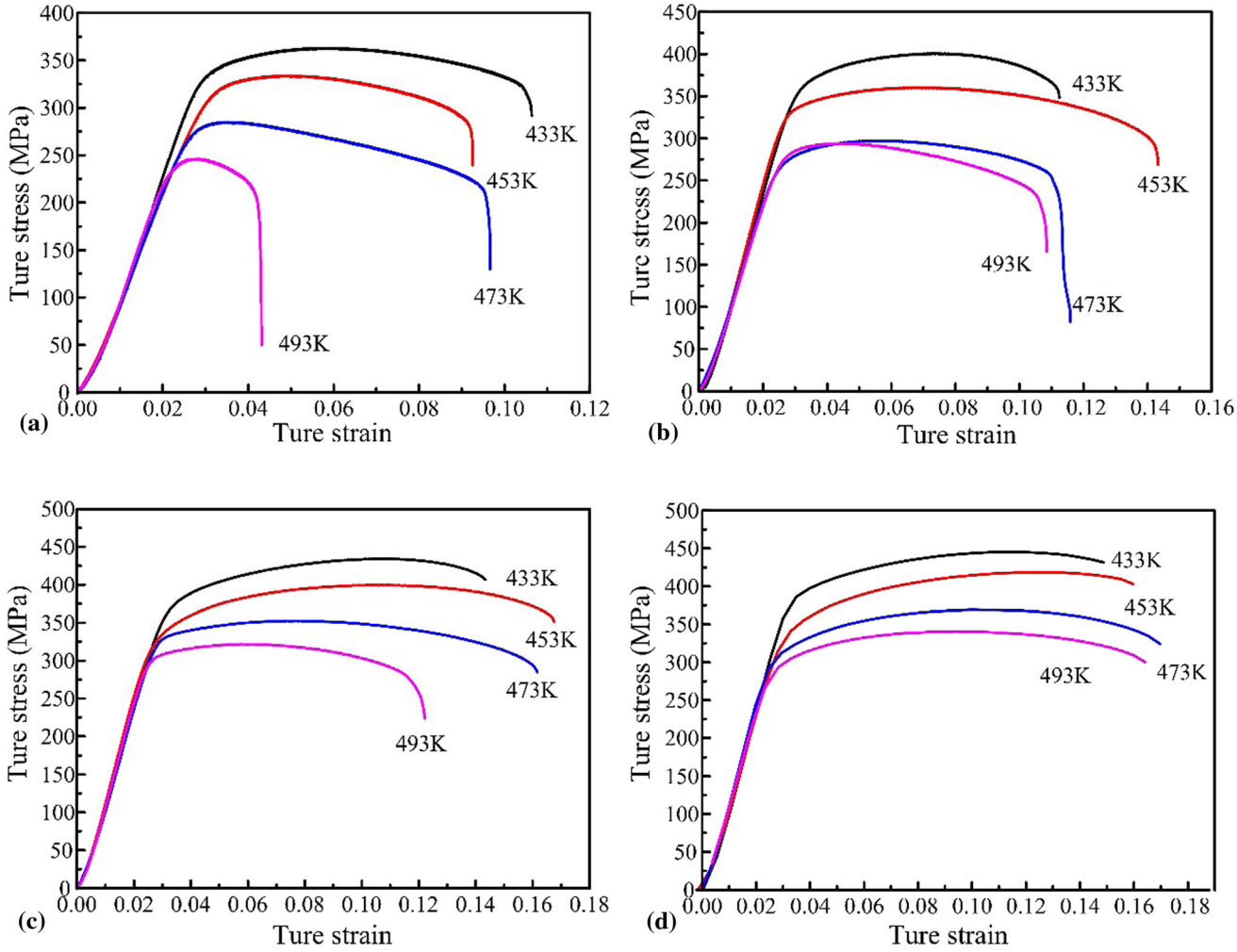

Fig. 2 True stress–strain curves of Al-Cu alloys at different temperature from 433 to 493 K with various strain rates: (a) 10^{-4} s^{-1}; (b) 10^{-3} s^{-1}; (c) 10^{-2} s^{-1} and (d) $10^{-1}s^{-1}$

Table 1 Data of the tensile experiment of the inoculated Al-Cu alloys by ZrCuAlNi metallic glass at various temperatures

	433, K		453, K		473, K		493, K	
$\dot{\varepsilon}$	σ_b, /MPa	δ_f, %	σ_b, MPa	δ_f, %	σ_b, MPa	δ_f, %	σ_b, MPa	δ_f, %
10^{-4}	343	11.2	317	9.7	275	10	239	4.36
10^{-3}	374	11.9	338	15.4	282	12	281	11.4
10^{-2}	394	15.4	364	18.2	330	17.5	305	12.3
10^{-1}	403	16	375	17.4	337	18.5	313	18

greater than those obtained for strain rates of 10^{-1} s^{-1}. This suggests that at elevated temperatures (specifically at 493 K), there is an increased tendency for θ′ precipitates to coarsen over time compared to lower temperatures (433 K). This could be attributed to the fact that higher temperatures can accelerate the diffusion process, which can allow for easier coarsening. Additionally, higher strain rates (specifically under conditions with a rate of deformation equaling or exceeding 10^{-1} s^{-1}) result in higher K values. This phenomenon can be attributed to dynamic aging precipitation effects on the growth rate of θ′ precipitate phases (Ref 28, 29). In the presence of high strain rate, there is a tendency for rapid growth of the θ' precipitates (Ref 29). Consequently, both deformation temperature and strain rate significantly influence the final size of θ' precipitates during tensile experiments.

In the field of metallurgy, precipitation strengthening is widely recognized as a strategy for enhancing mechanical properties, especially in Al-Cu alloys. During the stage of plastic deformation, θ' precipitates exhibit a stronger ability to hinder and accumulate dislocations (Ref 2, 26). This phenomenon not only enhances the capacity for dislocation storage but also leads to significant work hardening (Ref 30, 31). Furthermore, the precipitation strengthening mainly depends on the size of θ' precipitates, and smaller sizes can result in a more

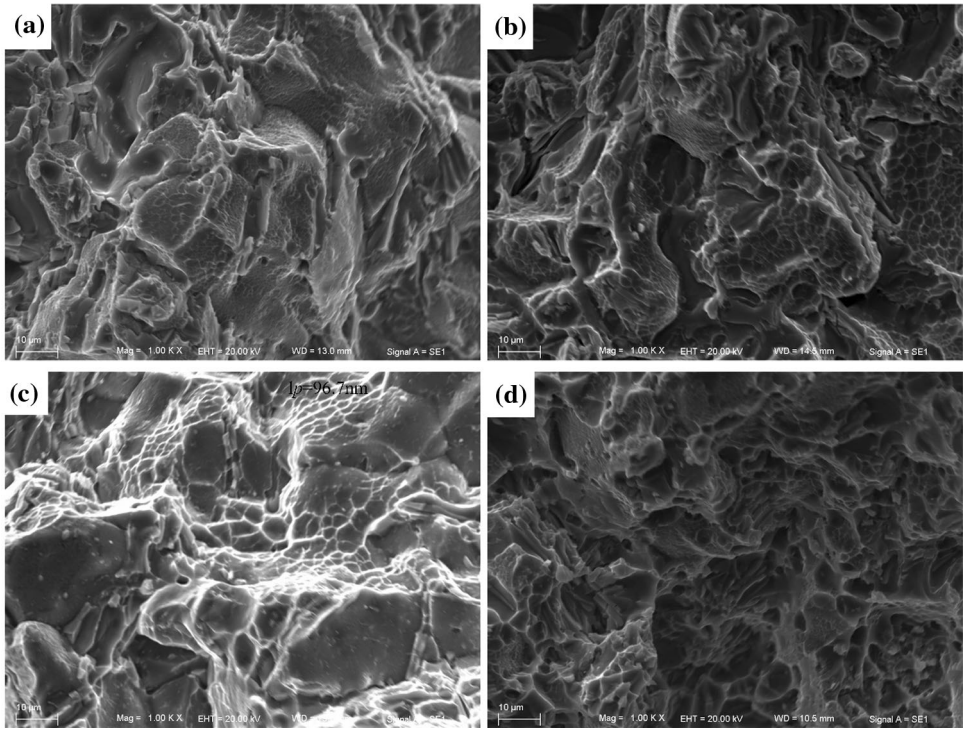

Fig. 3 SEM fractography of the studied Al-Cu alloy after tensile experiments under different conditions: (a) 10^{-4} s^{-1} and 433 K; (b) 10^{-1} s^{-1} and 433 K; (c) 10^{-4} s^{-1} and 493 K; (d) 10^{-1} s^{-1} and 493 K

prominent effect. Besides, work softening occurs due to dynamic recovery and recrystallization at elevated temperatures. Hence, the strain-hardening ability is the net value between work hardening and work softening in this paper. Figure 5 illustrates the strain-hardening characteristics of the Al-Cu alloys at elevated temperatures. Figure 5(a) shows the work-hardening rate Θ (dσ/dε) versus net flow stress ($\sigma - Y$), where Y is the (0.2% off-set) yield strength, during the plastic deformation at 10^{-1} s^{-1} with various elevated temperatures. The high initial Θ value rapidly decreased with the net flow stress gradually increased, and subsequently, the Θ value decreased at a slower rate eventually stabilizing at zero when the net flow stress reaches a certain threshold. It is evident that the Θ value increased when the temperature was lowered while fixing the net flow stress. With the increase in deformation temperature, the K value increases, and the size of θ′ precipitates increases, as depicted in Fig.4(b)and (d), resulting in a decrease in driving force for dislocation movement and consequently reducing the work-hardening rate, leading to a decrease in flow stress. Figure 5(b) illustrates the relationship between work-hardening rate Θ (dσ/dε) and net flow stress ($\sigma - Y$) during plastic deformation at 433 K under various strain rates. A similar trend of strain hardening can be observed. It is apparent that the Θ value increased with increase in strain rate while maintaining a fixed net flow stress level. With an increase in strain rate, although the K value also increases, lower strain rates allow more time for θ' precipitates to grow, as shown in Fig. 4(a) and (b), resulting in larger θ' precipitate sizes at low strain rates. As a result, precipitation strengthening effect weakens at lower strain rates, thereby reducing the overall flow stress level. Therefore, the change of θ' precipitates has a significant impact on high-temperature mechanical properties of Al-Cu alloys.

Concurrently, Fig. 2 vividly illustrates the influence of strain rate on the flow stress value. The strain-rate sensitivity exponent m can be mathematically represented as $m = \partial \ln \sigma / \partial \ln \dot{\varepsilon} = \partial \ln \sigma / \partial \ln \dot{\varepsilon}$. It can give better approximations to use peak stress as the representative flow stress. The findings indicate that at temperatures of 433, 453, 473 and 493 K, the corresponding m values are approximately 0.030, 0.034, 0.041 and 0.046, respectively. For common metal materials, m = 0.02-0.2; for many superplastic metal materials, m = 0.3-0.9. The strain velocity sensitivity m has a significant effect on the total strain from the beginning of necking to fracture. Commonly, the larger the m value, and the greater the possibility of high elongation. It can be found that with increase in deformation temperature, there is a gradual increase in the m value. Deforming at high strain rate with low m value typically indicates intragranular dislocation activity (Ref 32). Generally speaking, when $m > 0.3$ (or $m < 0.3$) under deformation conditions, it corresponds to grain boundary sliding processes (or dislocation creep processes) (Ref 32). Therefore, the deformation mechanism of the Al-Cu alloys at the elevated temperatures in this study is controlled by dislocation creep.

4. Conclusion

In this paper, the deformation behaviors of inculcated Al-Cu alloys were studied by uniaxial tensile tests under elevated temperatures with various strain rates. The peak stress increases with increase in strain rates from 10^{-4} to 1.0^{-1} s^{-1} or decrease in deformation temperatures from 433 to 493 K. The size of θ' precipitates increases with decrease in strain rates or increase in

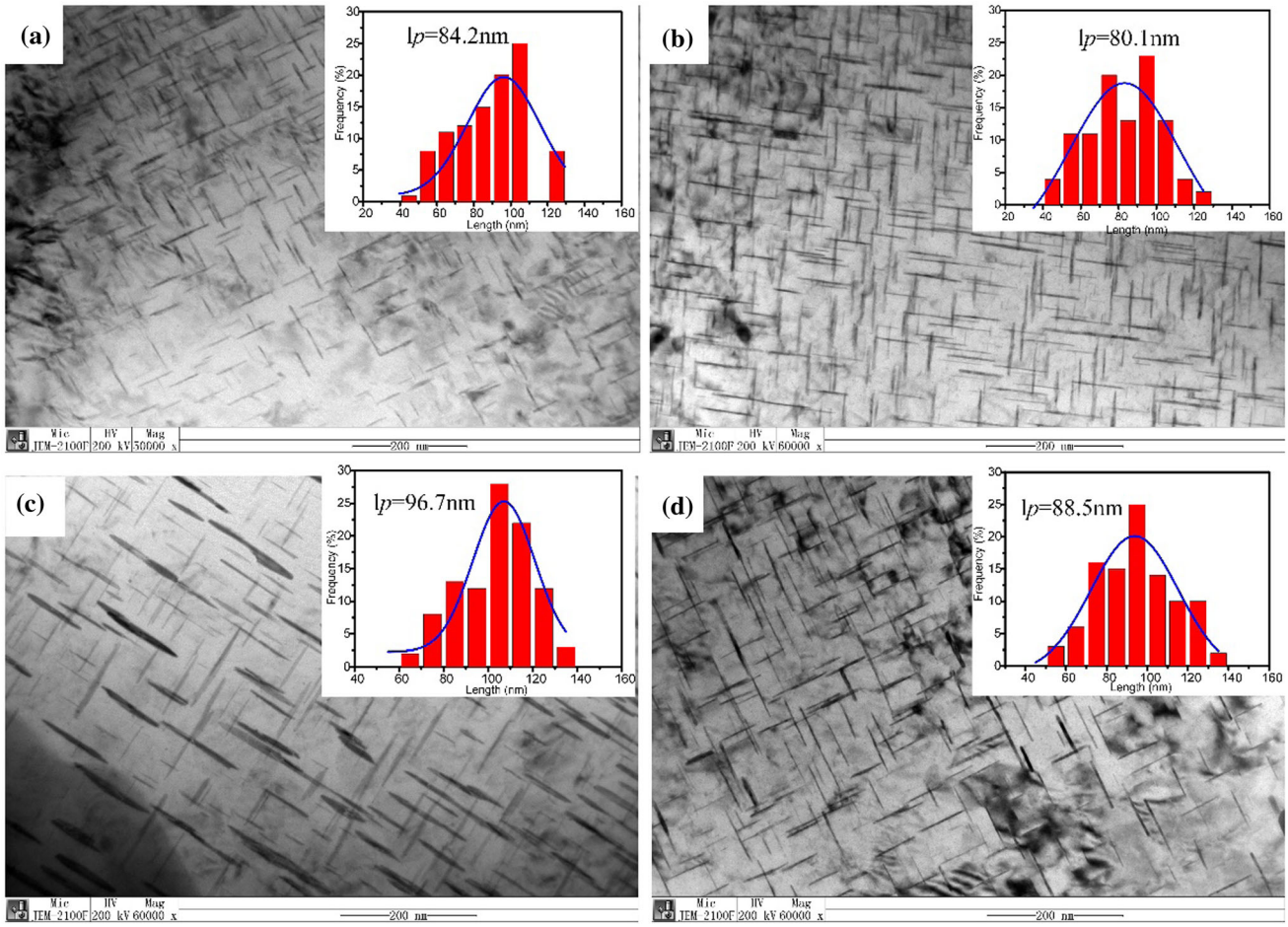

Fig. 4 TEM micrograph of the studied Al-Cu alloy after tensile experiments under different conditions: (a) 10^{-4} s^{-1} and 433 K; (b) 10^{-1} s^{-1} and 433 K; (c) 10^{-4} s^{-1} and 493 K; (d) 10^{-1} s^{-1} and 493 K

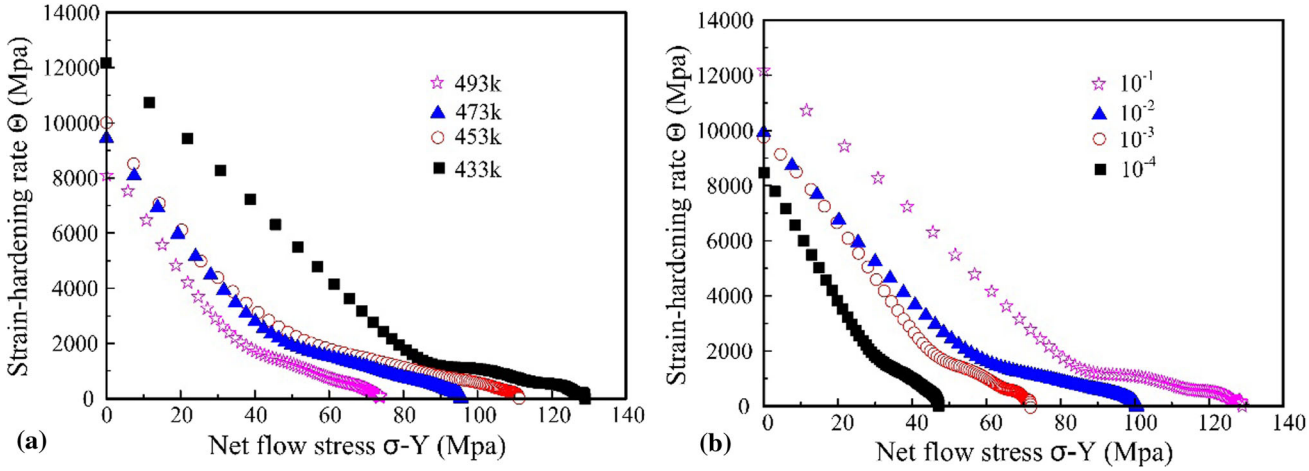

Fig. 5 Typical the strain-hardening rate (Θ)-net flow stress σ-Y curves under different conditions: (a) 10^{-1} s^{-1} and (b) 433 K

deformation temperatures, which can reduce work-hardening capacity during plastic deformation stage, thus reducing the flow stress level. The deformation mechanism of Al-Cu alloys at the elevated temperatures is controlled by dislocation creep in this paper.

Acknowledgments

This work is supported by the National Natural Science Foundation of China (No. 51801084), and Fundamental Research Funds for the Central Universities (B220203019).

References

1. L. Zhu, F. Qiu, Q. Zou, X. Han, S.L. Shu, H.Y. Yang, and Q.C. Jiang, Multiscale Design of α-Al, Eutectic Silicon and Mg_2Si Phases in Al-Si-Mg Alloy Manipulated by In Situ Nanosized Crystals, *Mater. Sci. Eng. A*, 2021, **802**, p 140627.
2. Z.H. Bai, F. Qiu, J.X. Chi, T. Zhang, and Q.C. Jiang, Microstructure Evolution and Mechanical Properties of Al-Cu Alloys Inoculated by FeBSi Metallic Glass, *Mater. Des.*, 2015, **67**, p 130-135.
3. Q. Li, F. Qiu, B.X. Dong, H.Y. Yang, S.L. Shu, M. Zha, and Q.C. Jiang, Investigation of the Influences of Ternary Mg Addition on the Solidification Microstructure and Mechanical Properties of As-Cast Al-10Si Alloys, *Mater. Sci. Eng. A*, 2020, **798**, p 140247.
4. T.S. Li, F. Qiu, B.X. Dong, R. Geng, and M. Zha, Role of Trace Nanoparticles in Establishing Fully Optimized Microstructure Configuration of Cold-Rolled Al Alloy, *Mater. Des.*, 2021, **206**, p 109743.
5. Q. Li, B.X. Dong, T.S. Liu, H.Y. Yang, and S.L. Shu, Insight into Solidification Microstructure Control by Trace TiCN–TiB_2 Particles for Yielding Fine-Tuned Nanoprecipitates in a Hypoeutectic Al–Si–Mg Alloy, *Mater. Sci. Eng. A*, 2021, **827**, p 142093.
6. A. Guinier, Structure of Age-Hardened Aluminium-Copper Alloys, *Nature*, 1938, **142**, p 569.
7. G.D. Preston, Structure of Age-Hardened Aluminium-Copper Alloys, *Nature*, 1938, **142**, p 570.
8. H. Liu, I. Papadimitriou, F.X. Lin, and J. LLorca, Precipitation During High Temperature Aging of Al-Cu Alloys: A Multiscale Analysis Based on First Principles Calculations, *Acta Mater.*, 2019, **167**, p 121-135.
9. L. Zhou, C.L. Wu, P. Xie, F.J. Niu, W.Q. Ming, K. Du, and J.H. Chen, A Hidden Precipitation Scenario of the θ′-Phase in Al-Cu Alloys, *J. Mater. Sci. Technol.*, 2021, **75**, p 126-138.
10. D. Li, K. Liu, J. Rakhmonov, and X.G. Chen, Enhanced Thermal Stability of Precipitates and Elevated-Temperature Properties via Microalloying with Transition Metals (Zr, V and Sc) in Al-Cu 224 Cast Alloys, *Mater. Sci. Eng. A*, 2021, **827**, p 142090.
11. L.Y. Cui, K. Liu, Z. Zhang, and X.G. Chen, Enhanced Elevated-Temperature Mechanical Properties of Hot-Rolled Al-Cu Alloys: Effect of Zirconium Addition and Homogenization, *J. Mater. Sci.*, 2023, **58**, p 11424-11439.
12. P. Hu, K. Liu, L. Pan, and X.G. Chen, Effect of Mg Microalloying on Elevated-Temperature Creep Resistance of Al-Cu 224 Cast Alloys, *Mater. Sci. Eng. A*, 2022, **851**, p 143649.
13. P. Hu, K. Liu, L. Pan, and X.G. Chen, Effect of Mg on Elevated-Temperature Low Cycle Fatigue and Thermo-Mechanical Fatigue Behaviors of Al-Cu Cast Alloys, *Mater. Sci. Eng. A*, 2023, **885**, p 145588.
14. P. Shower, J. Morris, D.W. Shin, B. Radhakrishnan, J. Poplawsky, and A. Shyam, Mechanisms for Stabilizing θ′ (Al_2Cu) Precipitates at Elevated Temperatures Investigated with Phase Field Modeling, *Materialia*, 2019, **6**, p 100335.
15. M.V. Petrik, Y.N. Gornostyrev, and P.A. Korzhavyi, Segregation of Alloying Elements to Stabilize θ′ Phase Interfaces in Al-Cu Based Alloys, *Scr. Mater.*, 2021, **202**, p 114006.
16. A. Shyam, S. Roy, D. Shin, J.D. Poplawsky, L.F. Allard, Y. Yamamoto, J.R. Morris, B. Mazumder, J.C. Idrobo, A. Rodriguez, T.R. Watkins, and J.A. Haynes, Elevated Temperature Microstructural Stability in Cast AlCuMnZr Alloys Through Solute Segregation, *Mater. Sci. Eng. A*, 2019, **765**, p 138279.
17. Y.Q. Chen, Z.Z. Zhang, Z. Chen, A. Tsalanidis, M. Weyland, S. Findlay, L.J. Allen, J.H. Li, N.V. Medhekar, and L. Bourgeois, The Enhanced Theta-Prime θ′ Precipitation in an Al-Cu Alloy with Trace Au Additions, *Acta Mater.*, 2017, **125**, p 340-350.
18. P. Shower, S. Roy, C.S. Hawkins, and A. Shyam, The Effects of Microstructural Stability on the Compressive Response of Two Cast Aluminum Alloys up to 300°C, *Mater. Sci. Eng. A*, 2017, **700**, p 519-529.
19. P. Shower, J.R. Morris, D. Shin, B. Radhakrishnan, L.F. Allard, and A. Shyam, Temperature-Dependent Stability of θ′-Al_2Cu Precipitates Investigated with Phase Field Simulations and Experiments, *Materialia*, 2019, **5**, p 100185.
20. M.V. Petrik, Y.N. Gornostyrev, and P.A. Korzhavyi, Point Defect Interactions with Guinier-Preston Zones in Al-Cu Based Alloys: Vacancy Mediated GPZ to θ′-Phase Transformation, *Scr. Mater.*, 2019, **165**, p 123-127.
21. Z.H. Bai, F. Qiu, X.X. Wu, Y.Y. Liu, and Q.C. Jiang, Age Hardening and Creep Resistance of Cast Al–Cu Alloy Modified by Praseodymium, *Mater. Charact.*, 2013, **86**, p 185-189.
22. D.M. Yao, Z.H. Bai, F. Qiu, Y.J. Li, and Q.C. Jiang, Effects of La on the Age Hardening Behavior and Precipitation Kinetics in the Cast Al–Cu Alloy, *J. Alloys Compd.*, 2012, **540**, p 154-158.
23. Z.H. Bai, F. Qiu, Y.Y. Liu, W. Zhou, and Q.C. Jiang, Age Hardening and Mechanical Properties of Cast Al-Cu Alloy Modified by La and Pr, *Adv. Eng. Mater.*, 2015, **17**, p 143-147.
24. D.M. Yao, W.G. Zhao, H.L. Zhao, F. Qiu, and Q.C. Jiang, High Creep Resistance Behavior of the Casting Al–Cu Alloy Modified by La, *Scr. Mater.*, 2009, **61**, p 1153-1156.
25. Z.H. Bai, F. Qiu, Y.Y. Liu, and Q.C. Jiang, Superior Strength and Ductility of the Al–Cu Alloys Inoculated by Zr-Based Metallic Glass at Elevated Temperatures, *Mater. Sci. Eng. A*, 2015, **645**, p 357-360.
26. L. Zhu, T.S. Liu, T.T. Duan, T.T. Li, F. Qiu, H.Y. Yang, Z.H. Bai, Y.Y. Liu, and Q.C. Jiang, Design of a New Al-Cu Alloy Manipulated by In-Situ Nanocrystals with Superior High Temperature Tensile Properties and Its Constitutive Equation, *Mater. Des.*, 2019, **181**, p 107945.
27. Z.H. Bai, F. Qiu, T. Zhang, and Q.C. Jiang, A New Approach to Refine Grains in Al Alloys, *Adv. Eng. Mater.*, 2015, **17**, p 796-801.
28. W.Z. Han, Y. Chen, A. Vinogradov, and C.R. Hutchinson, Dynamic Precipitation During Cyclic Deformation of an Underaged Al–Cu Alloy, *Mater. Sci. Eng. A*, 2011, **528**, p 7410-7416.
29. W.G. Zhao, H.Y. Wang, J.G. Wang, D.M. Yao, H.L. Zhao, and Q.C. Jiang, Effect of Nano-Scale Precipitates Growth on the Deformation Behavior of the Cast Coarse-Grained Al-Cu Alloy, *Adv. Eng. Mater.*, 2008, **10**, p 1114-1116.
30. S. Cheng, Y.H. Zhao, Y.T. Zhu, and E. Ma, Optimizing the Strength and Ductility of Fine Structured 2024 Al Alloy by Nano-Precipitation, *Acta Mater.*, 2007, **55**, p 5822-5832.
31. Y.H. Zhao, X.Z. Liao, S. Cheng, E. Ma, and Y.T. Zhu, Simultaneously Increasing the Ductility and Strength of Nanostructured Alloys, *Adv. Mater.*, 2006, **18**, p 2280-2283.
32. R. Panicker, A.H. Chokshi, R.K. Mishra, R. Verma, and P.E. Krajewski, Microstructural Evolution and Grain Boundary Sliding in a Superplastic Magnesium AZ31 Alloy, *Acta Mater.*, 2009, **57**, p 3683-3693.